ELSEVIER

Journal of Structural Geology 29 (2007) 1831–1842

JOURNAL OF STRUCTURAL GEOLOGY

www.elsevier.com/locate/jsg

Characterization of strike-slip fault–splay relationships in sandstone

Ghislain de Joussineau*, Ovunc Mutlu, Atilla Aydin, David D. Pollard

Rock Fracture Project, Department of Geological and Environmental Sciences, 450 Serra Mall, Building 320, Stanford University, Stanford, CA 94305, USA

Received 12 September 2006; received in revised form 9 August 2007; accepted 14 August 2007
Available online 1 September 2007

Abstract

We document the length and angular relationships between strike-slip faults and their splays. The data indicate that the maximum splay length is correlated to the fault length by a power law but shows little correlation with the fault slip magnitude. The kink angle between faults and their splays is small for isolated faults (average $\sim 20^\circ$) and systematically larger for mechanically interacting faults (average $\sim 50^\circ$). Analytical models predict that splay length decreases with increasing confinement under biaxial compression. 2D numerical models of isolated faults show that small kink angles correspond to small values of the angle between the fault and the maximum compression (β) whereas large kink angles require greater β values. Similar models of interacting faults confirm the critical role of β on the kink angles and suggest that fault overlap and fault separation can also induce important variations in the kink angles. Our results provide a basis for a better understanding of fault segment linkage via splaying process and for a better assessment of the maximum thickness of fault damage zones. The results may also help to predict the length and orientation of secondary faults formed by splaying associated with first order faults with resolvable slip magnitude in the subsurface.

Keywords: Splays; Strike-slip faults; Splay length; Kink angle; Cohesive end zone

1. Introduction

Splays, also called wing, tail, kink, horsetail and branch cracks, are dominantly opening-mode fractures formed in response to slip across shear fractures in brittle rocks such as sandstone (Cruikshank et al., 1991; Myers and Aydin, 2004), limestone (Rispoli, 1981; Fletcher and Pollard, 1981; Petit and Mattauer, 1995) and granite (Segall and Pollard, 1983; Granier, 1985), and in other natural materials such as ice (Wilson, 1960; Schulson, 2002; Kattenhorn and Marshall, 2006). They form due to tensile stress concentration at fault tips (Pollard and Segall, 1987; Martel et al., 1988), at fault plane irregularities such as bends, steps, or relay zones and at points of variable frictional properties along the fault surface (Cooke, 1997).

Splays may form a dense and well connected damage zone around strike-slip faults (Martel et al., 1988; Kim et al., 2003, 2004; Myers and Aydin, 2004; Flodin and Aydin, 2004b) and may enhance fault zone permeability with a large impact on fluid flow in the subsurface. They also play a critical role in the process of fault growth by segment linkage (Martel, 1990; Bürgmann et al., 1994; Peacock and Sanderson, 1995; Martel and Boger, 1998; de Joussineau and Aydin, in press) and have a strong influence on the formation and evolution of normal faults (McGrath and Davison, 1995; Davatzes and Aydin, 2003; Davatzes et al., 2003a,b) and strike-slip faults (Martel et al., 1988; Kelly et al., 1998; Myers and Aydin, 2004; Flodin and Aydin, 2004a; Kim et al., 2004). Accordingly, splays were the subject of many studies over the past few decades. In particular, the angular relationships between faults and their splays have been intensively studied experimentally and theoretically. In experiments, the kink angle between a fault and its splays was found to be influenced by the frictional properties of the faults, the remote stress field, the angle of the faults

* Corresponding author. Beicip-Franlab, 232 Avenue Napoléon Bonaparte, 92502 Rueil-Malmaison Cedex, France. Tel.: +33 1 47 08 80 44.
E-mail address: ghislain.dejoussineau@beicip.com (G.de Joussineau).

0191-8141/$ - see front matter © 2007 Elsevier Ltd. All rights reserved.
doi:10.1016/j.jsg.2007.08.006

to the maximum compressive stress or the stress perturbations induced by fault interaction (Brace and Bombolakis, 1963; Bombolakis, 1973; Nemat-Nasser and Horii, 1982; Horii and Nemat-Nasser, 1985; Barquins et al., 1991; Barquins and Petit, 1992; Du and Aydin, 1995; Chaker and Barquins, 1996). From a theoretical point of view, Linear Elastic Fracture Mechanics (LEFM) theory predicts a kink angle equal to 70.5° between a pure mode II (shearing) crack and its splays based on the maximum circumferential stress criterion (Erdogan and Sih, 1963; Ingraffea, 1987). However, kink angles much smaller than 70.5° are reported along natural faults with a shear offset and no evidence of opening perpendicular to the faults (Rispoli, 1981; Liu, 1983; Petit and Barquins, 1988; Martel, 1997). This discrepancy between theory and nature has been attributed to the fact that the LEFM theory implies a point of infinite stress concentration and infinite displacement gradient at the fault tips, which is unrealistic because natural materials cannot bear infinite stress. To overcome this stress singularity at fault tips, some authors introduced a zone of higher friction or cohesion near the tips of the fault models, named the cohesive end zone (Dugdale, 1960; Barenblatt, 1962). This modeling procedure reproduced the kink angles observed in nature (Martel, 1997; Willemse and Pollard, 1998; Davatzes and Aydin, 2003) and helped to explain the formation of a set of splays behind the fault tip which are often observed in outcrop (Cooke, 1997).

Even though the angular relationships between faults and splays have been widely studied, few investigations have dealt with the length relationships between shear fractures and their splays (Nemat-Nasser and Horii, 1982, 1984; Horii and Nemat-Nasser, 1985, 1986). These studies showed that the propagation and length of splays were influenced by the loading conditions (uniaxial/biaxial compression or tension–compression) and the magnitude of the maximum compressive stress. In particular, they demonstrated that splays could have a greater length that their parent shear fractures under favorable stress conditions. They also suggested a possible relationship between shear fracture length and splay length such that the longest shear fracture produced the longest splays in samples tested under the same loading conditions (Horii and Nemat-Nasser, 1986). However, to the best of our knowledge, no geological field data concerning the length relationships between faults and splays are available to compare with these results.

In this paper, we document the fault slip and length and the angular relationships between small faults (length < 100 m) and their splays in strike-slip fault networks exposed in the Valley of Fire State Park (SE Nevada, USA). We establish that the length of the longest splay produced by a fault is correlated to the fault length by a power law, but shows very little correlation to the fault slip magnitude. Also, we use analytical models to investigate the impact of boundary conditions on finite splay length. We identify two distinct fault configurations leading to different kink angle distributions, and use mechanical models of faults with a cohesive end zone to constrain the range of variation in the kink angles. The results obtained provide a means of estimating the maximum thickness of fault damage zones and the orientation and length of splay fractures around subsurface faults with detectable slip magnitude.

2. Geologic setting

The study area is the Valley of Fire State Park located in southeast Nevada, where the Jurassic Aztec Sandstone has spectacular exposures and forms the southwestern extremity of the Colorado Plateau Mesozoic sandstone deposits (Fig. 1). This aeolian sandstone is a fine to medium-grained quartz arenite with porosities around 25% and permeabilities up to several Darcys (Flodin et al., 2003). The Aztec Sandstone is divided into three sub-units based on rock color and related diagenetic history: the lower (red) unit, the middle (buff) unit and the upper (orange) unit (Carpenter and Carpenter, 1994; Eichhulb et al., 2004). The total thickness of the Aztec Sandstone in the study area ranges from 800 m to 1400 m. It is estimated that the Aztec Sandstone was buried at approximately 1500–2000 m at the beginning of the formation of the strike-slip faults, based on the stratigraphic column in the study area (Bohannon et al., 1993; Çakir et al., 1998).

Deformation occurred in several stages in the Valley of Fire. The first stage was an episode of compaction and shear deformation banding (Hill, 1989; Taylor et al., 1999; Myers and Aydin, 2004; Sternlof et al., 2005) associated with the Cretaceous Sevier orogeny (Bohannon, 1983). Joints overprinted the bands and, finally, a network of strike-slip faults formed during the Miocene Basin and Range extension (Myers, 1999; Fig. 1). The relative temporal relationship between normal faults accommodating extension and the predominantly strike-slip faults in Fig. 1 is controversial.

Regarding the formation of the apparent conjugate strike-slip fault patterns in Fig. 1, Flodin and Aydin (2004a) proposed that this system of left- and right- lateral strike-slip faults owes its existence to the sequential shearing of an initial joint zone, formation of splays, and subsequent shearing of the splays (Fig. 2). Flodin et al. (2005) studied the distribution of cataclastic fault rock along these strike-slip faults as a function of fault slip and measured their petrophysical properties in the laboratory. They concluded that the fault rock thickness generally increases with fault slip. Ahmadov et al. (2007) focused on the geometry and petrophysical properties of multiple slip surfaces commonly observed within the fault zones and evaluated their impact on fault permeability. They concluded that slip surfaces should be treated as partially filled planar features rather than open features. The present authors also have a separate work in progress (de Joussineau and Aydin, in press) dealing with the evolution of damage zone associated with the strike-slip faults in the same locality. Fig. 3, simplified from this manuscript, illustrates fault growth and damage zone evolution by segment linkage.

3. Methodology

Measurements were taken throughout the three units of the Aztec Sandstone of the Valley of Fire to establish a

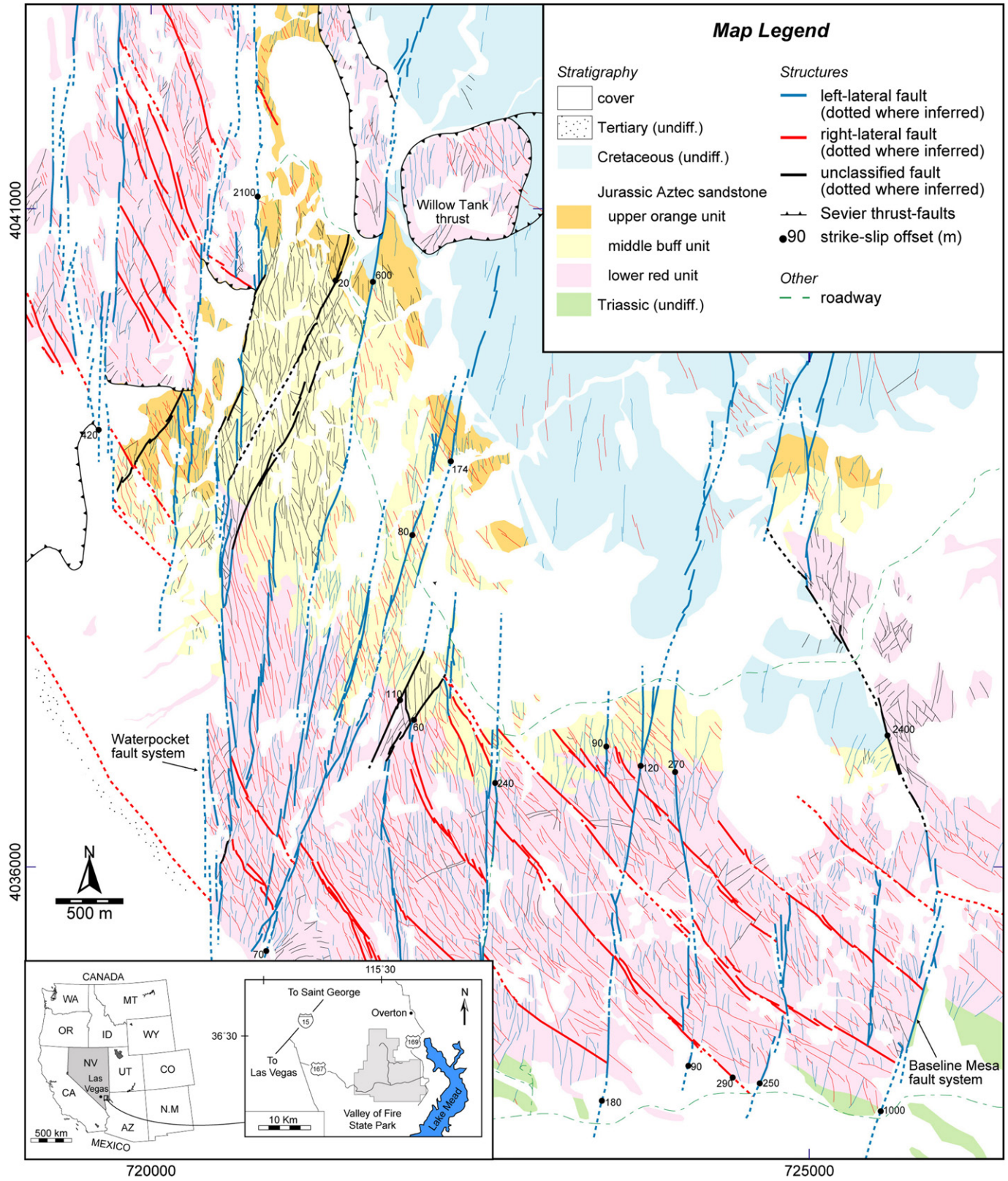

Fig. 1. Geographic location (inset) and fault map of the Valley of Fire State Park, SE Nevada (modified from Flodin and Aydin, 2004a).

comprehensive data set about the length and angular relationships between faults and their splays. The typical precision is ±1° for angular measurements and ±1% for length measurements.

To investigate the length relationships between faults and their splays, we identified cases where the propagation of the splays was not perturbed or stopped by any obstacle such as another fault, a joint or a deformation band. Accordingly, the

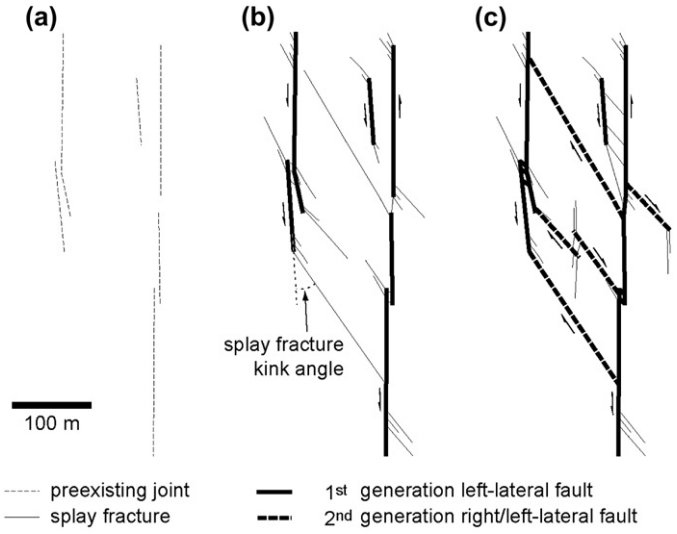

Fig. 2. Conceptual model for the evolution of the strike-slip fault networks in the Valley of Fire State Park, Nevada. (a) Pre-existing joints prior to, or at the earliest phase of, faulting. (b, c) Progressive stages of splay fracturing and sequential shearing of splay fractures that evolve into two sets of left- and right-lateral strike-slip faults in an apparent conjugate pattern. Simplified from Flodin and Aydin (2004a).

splays measured are the longest splays produced by the faults. Most traces of splays change orientation by less than 10°, and we measured their length along a straight line joining their base and tip. In the very few cases where the curvature of the splays was large enough to impact the length measurement, we divided the splays into several straight segments with different orientations and summed up the lengths of the segments to obtain the total length. In this case, the segment adjacent to the fault was used for the splay angle.

Many faults in the study area have striations that make a small angle to the strike of the fault indicating a dominant strike-slip component of the slip (Flodin and Aydin, 2004a). Accordingly, we considered the fault slip to be the separation determined based on the offsetting of markers such as deformation bands, dune boundaries or color bands. We measured the slip wherever possible, and when several measurements were made, the maximum separation was considered to be the maximum apparent slip along the faults.

4. Relationships between faults and their splays

4.1. Length relationships

To investigate the relationships between the length of the faults and the length of their longest splays (hereafter referred to as maximum splay length), we studied 135 left- and right-lateral faults ranging from 16 cm to 72 m in length. Fig. 4a shows that the maximum splay length (msl) is correlated to the parent fault length (pfl) by a nearly linear power law: $msl = 0.54pfl^{0.95}/R^2 = 0.79$. Fig. 4b shows the frequency distribution of msl/pfl ratios for the same fault population. Most of the msl/pfl ratios range from 0.2 to 1 and on average, the maximum splay length is equal to 60% of the fault length (msl/pfl = 0.6).

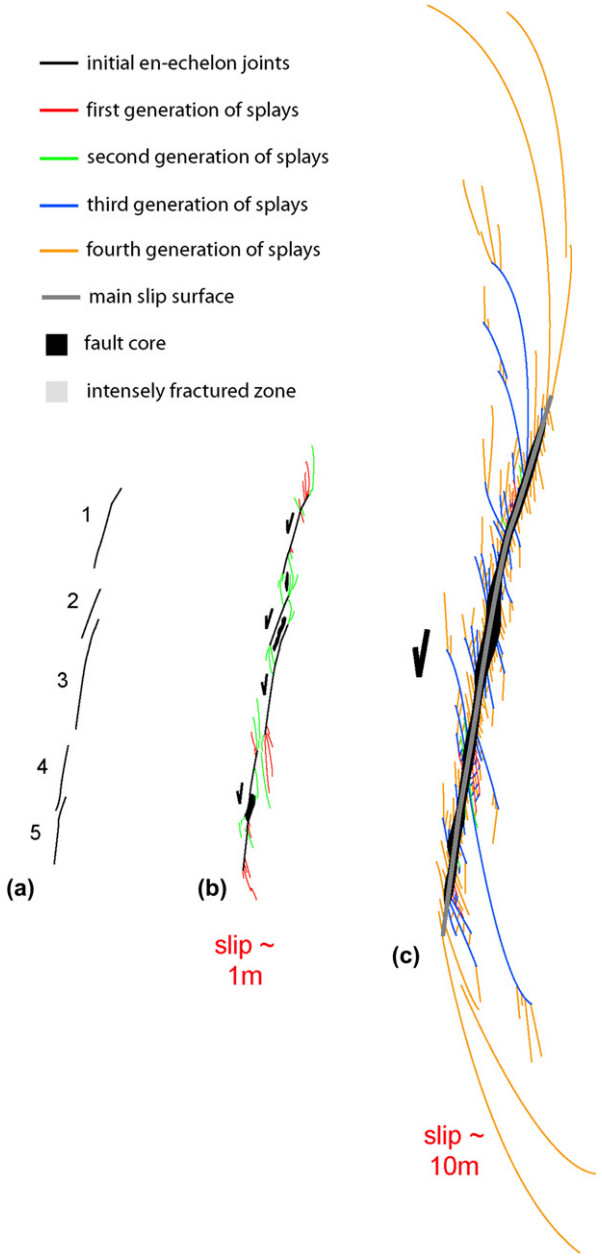

Fig. 3. Conceptual model for damage zone evolution with fault growth in the Valley of Fire State Park, Nevada. (a) Initial joint zone. (b, c) Progressive fault growth by segment linkage with the associated successive episodes of splay fracturing (different splay generations color-coded), as a function of the amount of fault slip. Simplified from de Joussineau and Aydin (in press).

Fig. 5 presents the relationships between the maximum splay length (msl) and the parent fault slip (pfs) for 73 of the faults where slip was measurable. Data show little correlation and are best fit by the following power law: $msl = 27.04pfs^{0.38}/R^2 = 0.40$.

4.2. Angular relationships

The kink angle is the acute angle between a fault and its splay in a clockwise sense for right-lateral shear and in a counter-clockwise sense for left-lateral shear. We measured

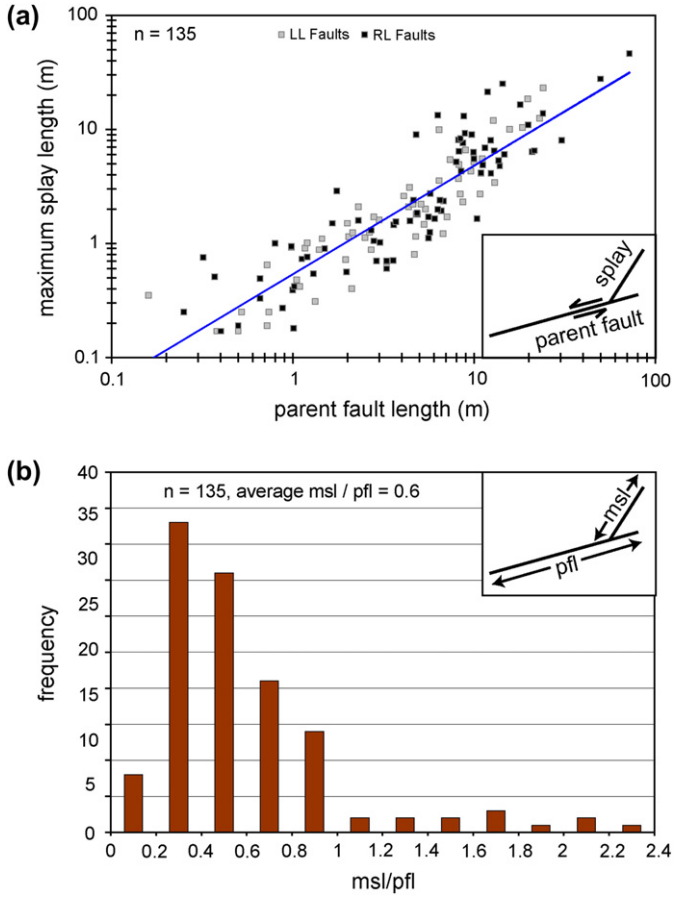

Fig. 4. (a) Relationships between maximum splay length and parent fault length. In the data, LL is for left-lateral and RL is for right-lateral, and the same convention is used in next figures. The best (power) fit to the data is shown. (b) Frequency versus the ratio of maximum splay length (msl) to parent fault length (pfl).

approximately 800 kink angles in the field and identified two fault configurations leading to different kink angle distributions. For the *isolated fault* configuration, a splay propagating from a fault tip ends in the host rock, away from any neighboring structure (Fig. 6a). In this case, most of the kink angles are less than 30° with an average value equal to 19° (Fig. 6b). For the *interacting fault* configuration, a splay connects its parent fault to a neighboring fault (Fig. 7a). The kink angle distribution differs from isolated faults, with most of the kink angles greater than 40° and an average value equal to 50° (Fig. 7b).

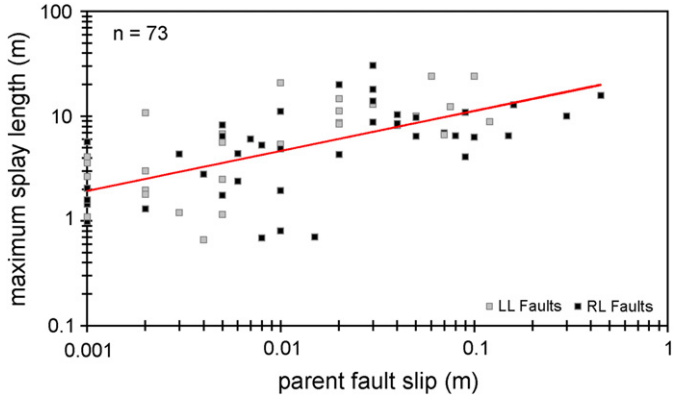

Fig. 5. Relationships between maximum splay length and parent fault slip. The best (power) fit to the data is shown.

5. Interpretations

5.1. Fault scaling relationships

As shown in Section 4.1, little correlation between maximum splay length and fault slip is observed whereas a clear relationship exists between maximum splay length and fault length. Fig. 8 proposes an interpretation for this observation by showing the relationships between the maximum fault slip (D) and the fault length (L) for 101 faults in the study area (including the 73 faults in Fig. 5). Data are poorly correlated and are best fit by the following power law: $D = 0.10L^{1.25}/R^2 = 0.48$. The fact that fault length is poorly correlated to fault slip may explain why maximum splay length, while strongly correlated to fault length, shows little correlation with fault slip.

Several factors may be responsible for the complex $D-L$ relationships in the study area. First, uncertainty about the determination of fault slip may exist. Slip was measured in locations where displaced markers were found and the maximum slip observed was considered to be the maximum slip along the faults. However, slip may be larger in other locations along the faults where no markers are present. This would influence the distribution of the slip values plotted in Figs. 5 and 8. Second, the faults in the Valley of Fire grew by segment linkage (Myers and Aydin, 2004; de Joussineau and Aydin, in press), implying episodes of interaction between neighboring fault segments during the process of fault development. This phenomenon has been proposed to influence the slip distribution along the faults and consequently the $D-L$ relationships. Indeed, although compilations propose linear or power law $D-L$ relationships (Cowie and Scholz, 1992a; Dawers et al., 1993; Schlische et al., 1996), and models based on elastic-plastic fracture mechanics provide the basis for constant $D-L$ ratios (Cowie and Scholz, 1992b), it has been shown that for faults growing by segment linkage, the $D-L$ relationships were affected by the degree of linkage between the segments composing the fault systems (Peacock and Sanderson, 1991; Cartwright et al., 1995; Gupta and Scholz, 2000; Mansfield and Cartwright, 2001 for normal faults; Peacock, 1991 for strike-slip faults).

5.2. Analytical investigation of splay length

In the following, we use analytical models to study the impact of the loading conditions on the finite length of splays propagating from frictional faults. Cotterell and Rice (1980) proposed an analytical solution to calculate the stress intensity factors, K_I and K_{II} at the tips of a splay crack. Their solution is valid for a parent fault subjected to either mode I or mode II loading, but assumes that the fault is frictionless. Here we consider the same problem, but for faults with friction. Horii and

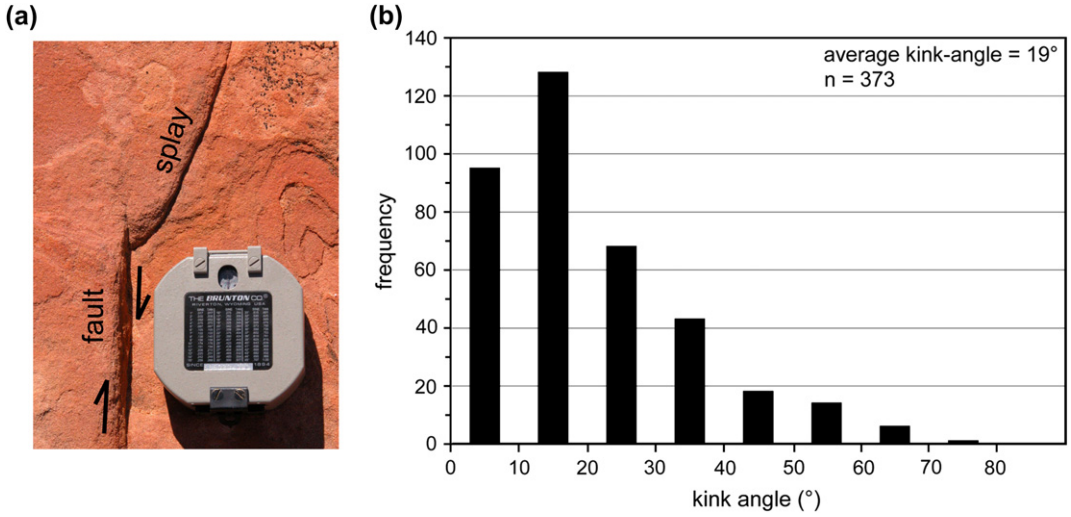

Fig. 6. (a) Photograph of an isolated fault configuration. (b) Corresponding kink angle distribution.

Nemat-Nasser (1983; 1986) provided an exact solution for a splay crack originating from a single two dimensional fault with friction and cohesion. This solution is derived from the stress potentials formulated by Muskhelisvili (1953) and expressed in terms of singular integral equations. By considering the splay cracks as straight fractures rather than curved ones, a very simple, closed form solution is obtained. This closed form solution is verified against the complete numerical solution and provides good estimates of the stress intensity factors for both small and large splay lengths (Horii and Nemat-Nasser, 1986). In this solution, the splitting force F acting on the splay crack can be calculated by estimating the driving shear stress $\tau*$ on the pre-existing fault, as follows:

$$F = 2c\tau* \tag{1}$$

$$\tau* = -0.5(\sigma_1 - \sigma_3)\sin(2\beta) - \text{cohesion} + 0.5\mu[\sigma_1 + \sigma_3 - (\sigma_1 - \sigma_3)\cos(2\beta)] \tag{2}$$

where c is the half-length of the fault, μ is the coefficient of friction, σ_1 and σ_3 are the maximum and minimum compressive stresses, respectively, and β is the angle between the fault and σ_1 (Fig. 9a).

Considering the effect of the far-field stresses σ_1 and σ_3, the mode I stress intensity factor at the tip of the splay crack is estimated by:

$$K_I = 2c\tau^* \frac{\sin(\alpha)}{\sqrt{\pi(\lambda + 0.27c)}} + \frac{\sqrt{\pi\lambda}}{2} [\sigma_1 + \sigma_3 - (\sigma_1 - \sigma_3)\cos 2(\alpha - \beta)] \tag{3}$$

where α is the kink angle between the fault and its splay and λ is the splay length (Fig. 9a).

For an opening-mode splay crack, the maximum splay length is obtained by equating the value of K_I in eq. (3) to the critical stress intensity factor K_{IC}. In the following, K_{IC} is equal to 0.28 MPa.m$^{1/2}$, consistent with aeolian sandstones (see values in Atkinson, 1987).

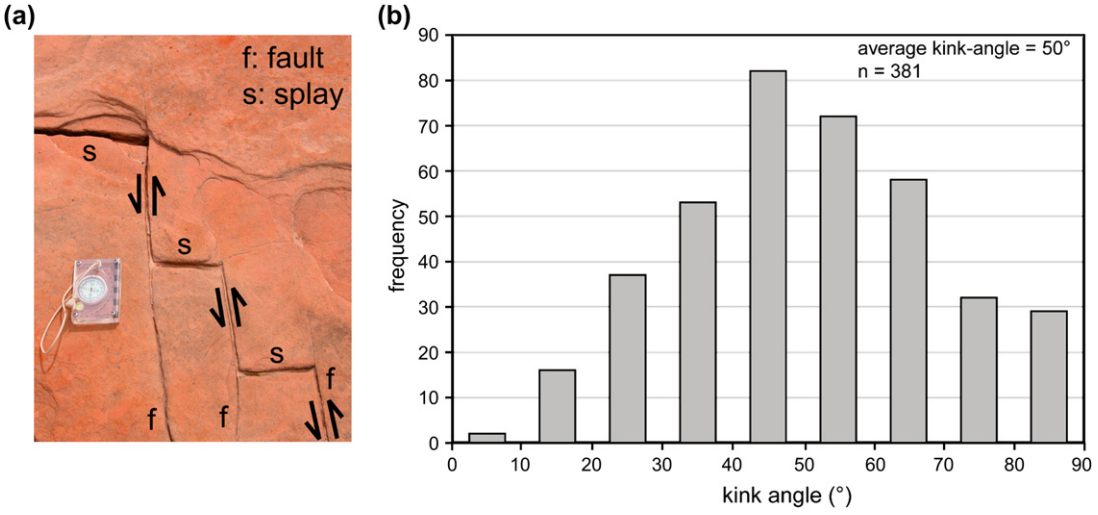

Fig. 7. (a) Photograph of interacting fault configurations. (b) Corresponding kink angle distribution.

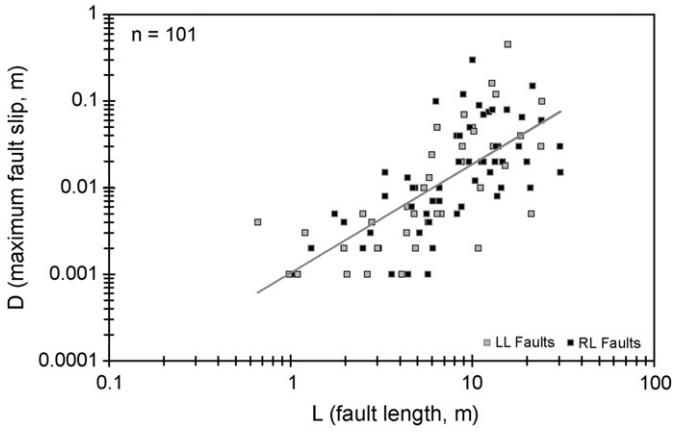

Fig. 8. Relationships between fault length (L) and maximum fault slip (D) for faults in the study area. The best (power) fit to the data is shown.

Fig. 9b and c show the variations of the normalized mode I stress intensity factor (K_I normalized $= K_I\sigma_1/\sqrt{\pi c}$) at the tip of a splay crack as a function of λ/c, for different stress ratios and fault configurations. The horizontal line in these figures marks the normalized critical Mode I stress intensity factor (K_{IC} normalized). The maximum length reached by the splays is found at the intersection between this line and the different curves.

Fig. 9b and c show that K_I decreases continuously as the splay length increases. Furthermore, the lateral confining stress σ_3 has an important impact on splay length. For uniaxial compression ($\sigma_3/\sigma_1 = 0$), the splay length tends to infinity. However, when a confining pressure exists ($\sigma_3 > 0$), the splay length is finite and decreases notably with increasing σ_3/σ_1. Finally, the different fault geometries in Fig. 9b and c lead to different splay lengths for similar loading conditions. This suggests that both the angle β between the fault and σ_1 and the kink angle α influence splay length.

These model results indicate how the splay length may be affected by the loading conditions, but are for the case when splays form in one event, which cannot be directly compared with the field situation where splays propagate in several events through heterogeneous rocks.

5.3. Mechanical constrains on kink angles

To interpret the variations in the kink angle distributions measured in the field (Figs. 6b and 7b), we investigated models of faults using a 2D boundary element method that included a complementarity algorithm for friction. Fundamentals and advantages of this algorithm for modeling frictional contact problems are described in Mutlu and Pollard (2006), where the algorithm satisfactorily reproduces kink angles published in previous studies (Martel, 1997; Willemse and Pollard, 1998).

The fault models are based on the cohesive end zone concept, which postulates that a zone of greater friction or cohesion exists near fault tips relative to other parts of the faults (Dugdale, 1960; Barenblatt, 1962). In this contribution, we follow the approach by Cooke (1997) in that our faults have a central part with a constant friction coefficient (equal to 0.4)

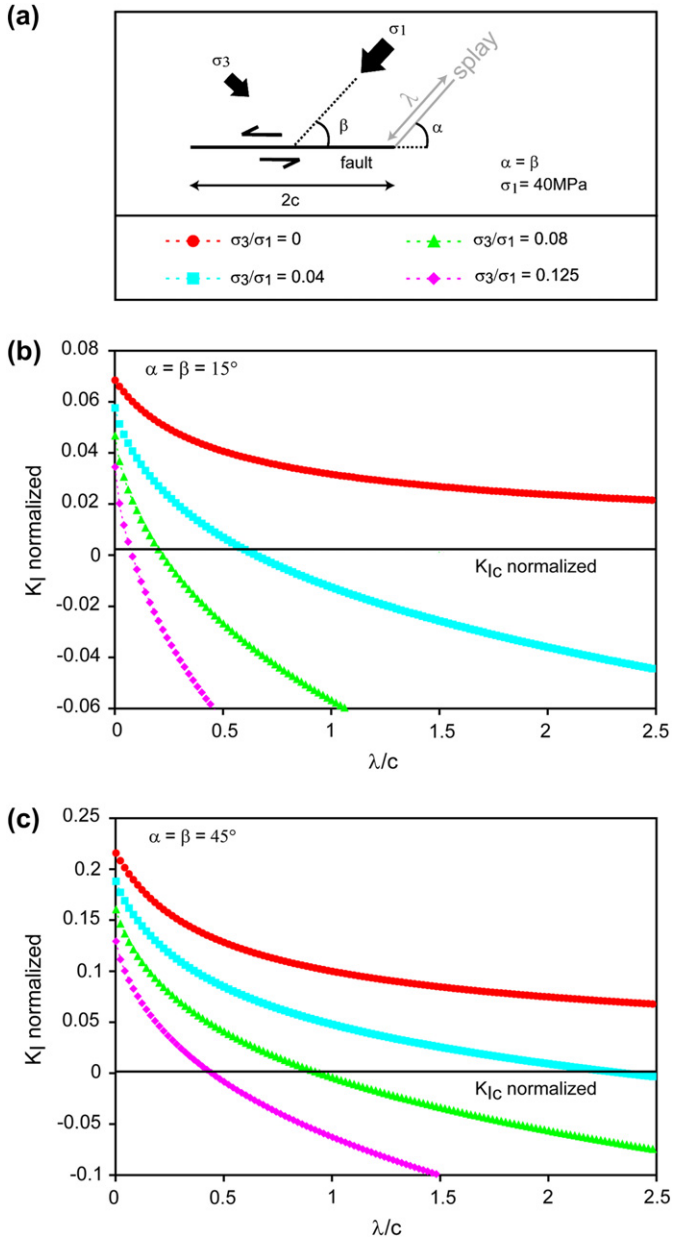

Fig. 9. (a) Fault configuration and symbols corresponding to various σ_3/σ_1 ratios; (b,c) Plots showing the relationships between K_I normalized and the ratio λ/c of splay length over the half-length of the fault for (b) $\alpha = \beta = 15°$ and (c) $\alpha = \beta = 45°$.

and a cohesive end zone with greater friction coefficient (equal to 0.9). We tested two different sizes of the cohesive end zone (cez $= 0.05L$ and cez $= 0.1L$ where L is the fault length). These sizes of the cohesive end zone are consistent with previous works. For example, Cowie and Scholz (1992b) developed a ratio of the cohesive end zone size to the fault length of 0.1 (i.e. $0.1L$ in our case) based on slip distribution data. Cooke (1997) used the same size for the cohesive end zone in her models. More recently, Wilkins and Schultz (2005) compiled data from the Landers, Hector Mine, and Izmit earthquakes to propose that the ratio of the cohesive end zone size to the fault length falls in the range of 0.07 to 0.225.

The maximum circumferential stress ($\sigma_{\theta\theta}$) criterion is used to calculate the kink angles. This criterion assumes that the location of the maximum circumferential stress at a fault tip determines the initial kink angle (Erdogan and Sih, 1963; Cotterell and Rice, 1980). We computed $\sigma_{\theta\theta}$ around the point where the central zone meets the cohesive end zone, at a radial distance $r = 0.0075L$.

In the modeling experiments, Young's modulus = 20 GPa and Poisson's ratio = 0.2, consistent with properties of sandstone (Atkinson, 1987). We tested the faults under biaxial compression in plane strain by setting the maximum compressive stress $\sigma_1 = 40$ MPa, consistent with σ_H values at 1500–2000 m depth in strike-slip environments (Engelder, 1993). We varied the minimum compressive stress, σ_3, from 0 to 25 MPa in models of isolated faults, again consistent with strike-slip environments, and set it to 5 MPa in models of interacting faults.

5.3.1. Isolated faults

Fig. 10 shows the relationships between the kink angle α and the angle β between the fault and σ_1 for isolated faults (see fault configuration in Fig. 10a). Little difference exists between the models with short (Fig. 10b) or long (Fig. 10c) cohesive end zones. For σ_3/σ_1 ratios equal to or less than 0.375, the kink angle α increases markedly as β increases from ~15° to ~25°, then is approximately constant until β reaches 55° to 65°. In all these situations, the central zone (and the end zone for cases with no or very little lateral confinement) of the faults accommodates slip. Also, σ_3 is a tensile stress at the limit between the central zone and the cohesive end zone, allowing splay propagation. When β exceeds 55–65°, slip is inhibited and $\alpha = \beta$, leading to unfavorable situations for splay propagation.

For greater σ_3/σ_1 ratios (0.5 and 0.625), the lateral compression prevents the faults from slipping and $\alpha = \beta$. No tensile stresses develop between the central zone and the cohesive end zone, preventing the formation of splays.

Only the stress conditions with little or no lateral confinement ($\sigma_3/\sigma_1 = 0$ and $\sigma_3/\sigma_1 = 0.125$) lead to a sufficient range of kink angles (i.e. ~5° to ~75°) to explain the distributions in Fig. 6b, whereas models with greater σ_3/σ_1 ratios do not predict kink angles larger than ~60° for slipping faults. Small kink angles (≤15°) correspond to situations where β is less than 15° and large kink angles (up to 75°) require greater values of β.

We note that the first three or four data points in the curve corresponding to the case where $\sigma_3/\sigma_1 = 0$ indicate much smaller kink angles than for the other models tested. This may reflect a tendency for nearly in-plane fracture propagation as mode I cracks. The results in Fig. 10 are consistent with results of simulations in previous models by Martel (1997) and Davatzes and Aydin (2003).

5.3.2. Interacting faults

The configuration of interacting faults includes two parallel faults with equal length L (Fig. 11a). Based on the case of an isolated fault, we set σ_3 to 5 MPa and the cohesive end zone to

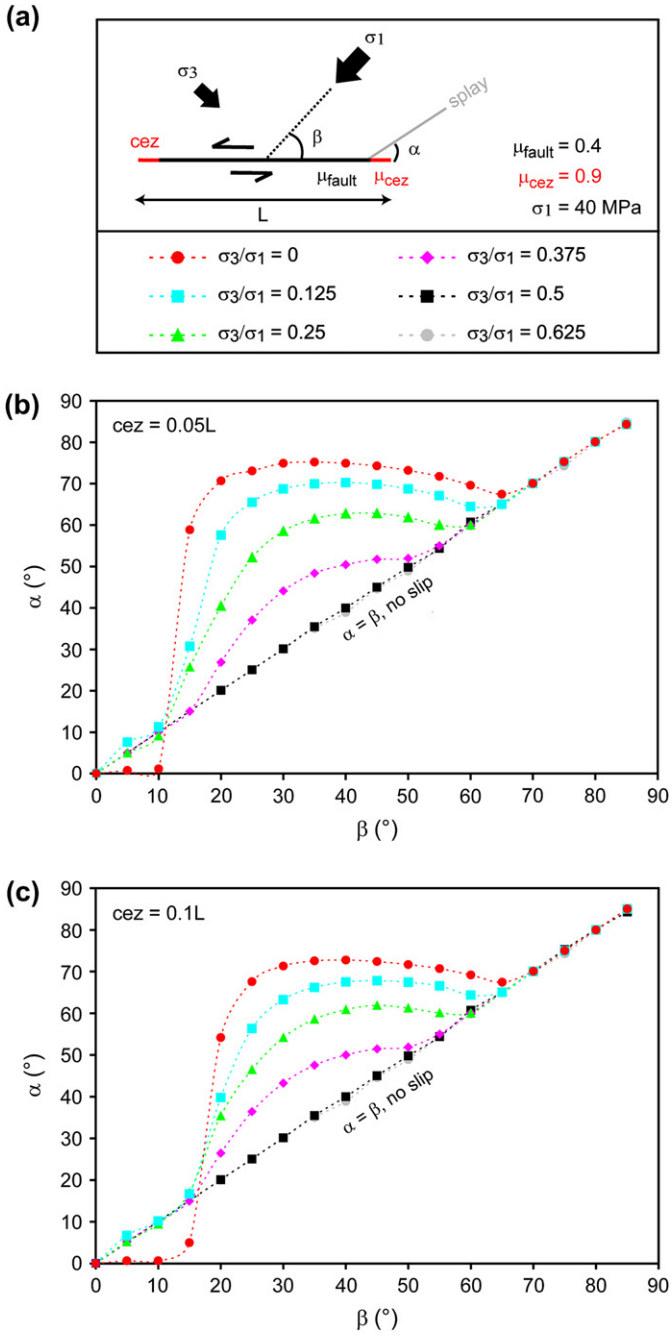

Fig. 10. (a) Fault configuration and symbols corresponding to various σ_3/σ_1 ratios; (b,c) Plots showing the relationships between the kink angle α and the angle β between the fault and σ_1 for two sizes of the cohesive end zone (b: cez = 0.05L, c: cez = 0.1L).

0.1L. This combination of parameters accounts for the kink angle distribution in Fig. 6b. All other parameters are the same as those used for isolated faults. The ranges of values for fault overlap (Fig. 11b) and fault separation (Fig. 11c) in these simulations are based on field observations in the study area.

First, we investigate the role of fault overlap "o" in changing the kink angle α with constant fault separation equal to 0.1L (Fig. 11b). "o" is a function of the fault length L and

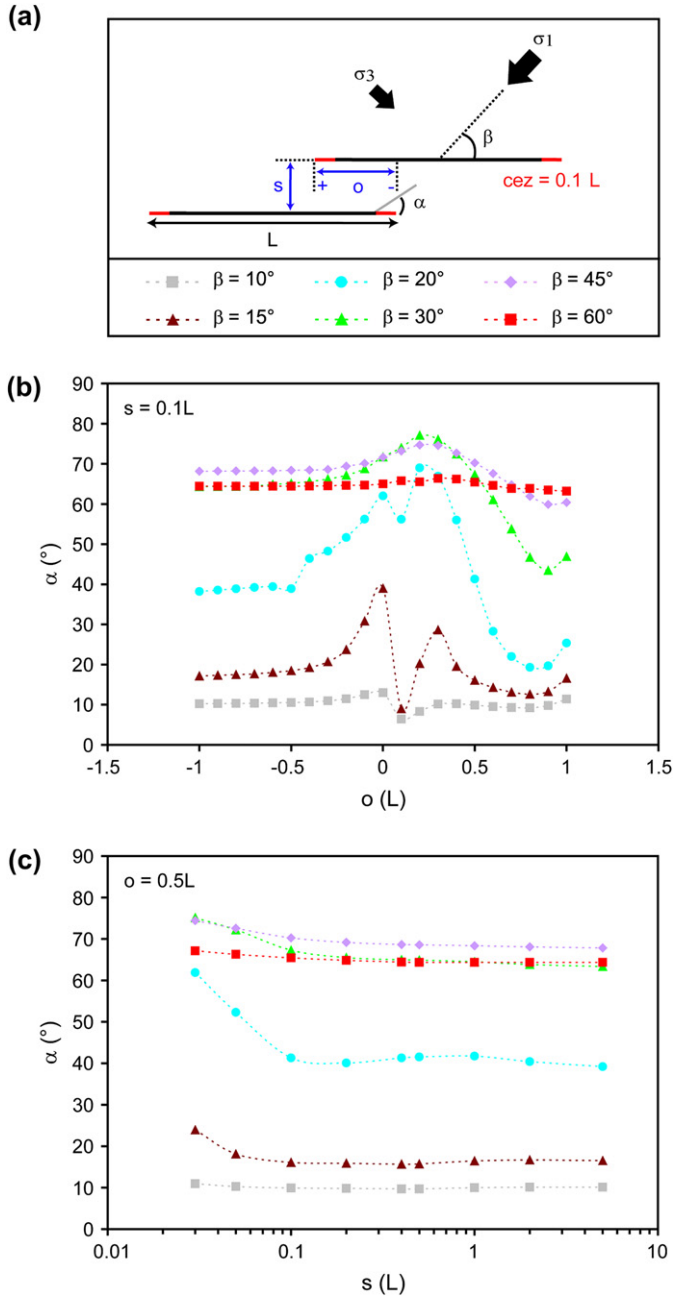

Fig. 11. (a) Fault configuration and symbols corresponding to various β values; Plots showing the relationships between (b) the kink angle α and the fault overlap "o" and (c) α and the fault separation "s".

negative values of "o" correspond to underlapping faults (i.e. faults with stepovers in which they are separated parallel as well as perpendicular to strike), whereas positive values of "o" correspond to overlapping faults.

When "o" is less than $-0.5L$, the kink angles are constant and comparable to kink angles for isolated faults because faults are too far away to interact. When "o" is greater than $-0.5L$, two situations occur depending on β. If β is equal to or more than 30°, α increases with "o" to reach a maximum for $o = 0.2L$. Then α decreases while "o" increases from $0.2L$ to $0.8L$, and finally α becomes constant or increases slightly when "o" is greater than $0.8L$. If β is less than 30°, the kink angles show variations similar to the previous case where β is larger except for $o = 0.1L$, where the kink angles decrease noticeably. The variations in the kink angles with fault overlap are significant if β is in the range of 15–30° but not if β is 45° or greater because of reduced fault slip.

In all these models, when β is equal to or greater than 15°, σ_3 is a tensile stress near the point where the central zone meets the cohesive end zone, allowing splay propagation. The predicted α values for β in the range of 15° to 30° have a distribution similar to field values (Fig. 7b) with kink angles ranging from ~5° to ~80° and the majority greater than 40°. However, no single simulated β value yields the observed range of kink angles. This suggests that fault configurations with different β values existed during splay development, possibly due to variations in initial fault trends or local perturbations of stress trajectories through time as the fracture patterns developed.

Second, we investigate the role of the fault separation "s" in changing the kink angle in experiments with constant fault overlap equal to $0.5L$. The results obtained indicate that the fault separation has less effect on the kink angle than the fault overlap. Regardless of β values, the kink angle decreases when "s" increases from $0.03L$ to $0.1L$, but becomes almost constant when "s" is larger than $0.1L$ (Fig. 11c). For such values of "s", the kink angles are comparable to kink angles for isolated faults. The magnitude of variation of the kink angles is largest when β is 20° but is almost negligible when β is 10° or 60°, because of very limited fault slip.

6. Application to damage zone thickness and the prediction of secondary faults

The splay length and angular distribution data sets may enable one to estimate how far and in which direction splays propagate from faults. Assuming that splays are initially nearly straight mode-I fractures, one can establish the following relationship between the splay length λ, the kink angle α, and the distance "x" that the splays propagate in the direction perpendicular to the faults: $x = \lambda \sin\alpha$ (Fig. 12). In the study area, the average splay length is 60% of the fault length (Fig. 4b): $\lambda \sim 0.6L$ where L is the fault length. For isolated

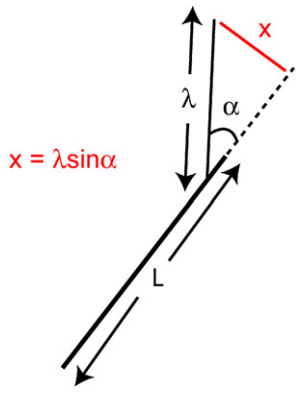

Fig. 12. Relationships between the splay length λ, the kink angle α and the distance "x" perpendicular to the fault to which the splays propagates.

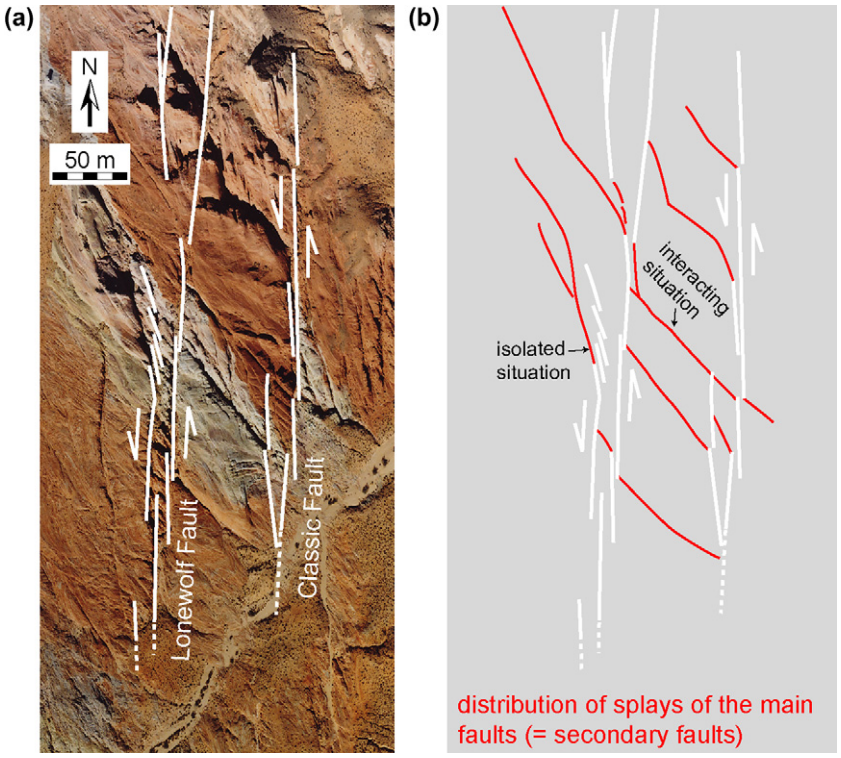

Fig. 13. (a) Geometry and segmentation of two main left-lateral faults systems in the study area, the Lonewolf Fault and the Classic Fault, shown in an aerial photograph. (b) Distribution and geometrical characteristics of the main splays (=secondary faults) of these faults. Examples of isolated and interacting fault situations are indicated in the figure.

faults, the average kink angle α is 19° (Fig. 6b), so $x \sim 0.2L$. This result indicates that on average, a splay propagating from an isolated fault reaches a distance "x" equal to 20% of the fault length. This may help in predicting the maximum thickness of fault damage zones in the case of faults developed by sequential shearing as in the study area (Myers and Aydin, 2004). For such faults, the damage zones may be constructed from splays (de Joussineau and Aydin, in press), implying that their maximum width is defined by the length and orientation properties of the longest splays emanating from the faults. Also, by proposing a means of estimating the length and orientation of splays in the tip region of fault segments, we provide a basis for a better understanding of the phenomenon of fault segment linkage by the way of splays.

Results of this study may also assist predicting the characteristics of secondary faults with displacements that are not detectable in seismic data, but are associated with faults with resolvable slip magnitude. Based on the length and arrangement in terms of overlap and separation of resolvable fault segments inferred from the seismic data, one may estimate whether these segments are likely to interact with their neighbors or not. Once a decision is made concerning the presence of "isolated" or "interacting" fault geometries, the fault architecture, and the length and angular relationships presented in this paper may be used to infer the location (segment tips), length and orientation of the main splays of the faults (Fig. 13). Fig. 13a shows the architecture of the Lonewolf Fault and the Classic Fault, two large faults with 80 m and 175 m slip, respectively. The architecture of these two fault systems, combined with the knowledge gained from the analysis of the fault–splay relationships, could allow one to determine the location and geometrical properties of the longest splays (main secondary faults) along the faults. Indeed, these main splays, shown in Fig. 13b, are located at the tip of the main fault segments, and have length and orientation properties (checked in the field) that satisfy the length and angular fault–splay relationships described in this paper. In particular, the kink angles in Fig. 13b are large where fault segments interact and are small for isolated faults.

The large fault splays are important because they increase the connectivity of the fault networks at a scale of 100 m. Furthermore, in the study area, they typically accommodate several meters of slip and may have well-developed and continuous cores with low permeability (Flodin et al., 2005). Consequently, if present in the subsurface, they would possibly compartmentalize this potential reservoir.

Caution is required when applying the results of the length and angular fault–splay analysis for this study area to different regions because splay length may be influenced by the loading conditions, implying that faults with similar length may produce shorter or longer splays depending on the local stress state.

7. Conclusions

We documented the length and angular relationships between strike-slip faults and their splays in the Valley of Fire State Park in SE Nevada. The length of the longest splays is

correlated to the fault length by a power law and, on average, is 60% of the fault length. Little correlation is found between splay length and fault slip magnitude, possibly because fault growth by segment linkage affects the slip distribution along the faults. Two distinct angular relationships between faults and splays exist depending on the fault configuration. In the isolated fault configuration, where splays propagating from a fault do not interfere with a neighboring fault, most kink angles are less than 30° with an average of 19°. In the interacting fault configuration, where splays propagating from a fault connect to a neighboring fault, most kink angles are more than 40° with an average value of 50°.

We used analytical models to test the influence of the loading conditions on splay length. Under uniaxial compression, the splay length tends to infinity. Under biaxial compression, the splay length is finite and depends on the stress ratio σ_3/σ_1. When this ratio increases, splay length decreases. Furthermore, different fault geometries yield different splay lengths for similar loading conditions, suggesting that both the angle β between the fault and σ_1 and the kink angle α influence the splay length.

We also used a 2D mechanical model to investigate the angular relationships between faults and splays established in the field. Models of isolated faults under plane strain conditions show that small kink angles correspond to a situation where faults make a small angle (β) with the remote maximum compressive stress, whereas large kink angles correspond to greater β values. Models of interacting faults show that, in addition to the important role of β, fault overlap and fault separation can induce important variations in the kink angle, which could explain the variety of kink angles measured in the field.

The knowledge acquired in terms of length and angular relationships between faults and their splays allows one to envision how far and in which direction splays may propagate from their parent faults. This may help to estimate the maximum thickness of fault damage zones, and provides a basis for a better understanding of fault segment linkage. Finally, it may permit the prediction of the length and orientation of unresolvable secondary faults associated with large faults that have resolvable slip magnitude in the subsurface.

Acknowledgments

We acknowledge support from the Department of Energy, Basic Energy Sciences, Geosciences Research Program (Grant #DE-FG03-94ER14462 to Atilla Aydin and David D. Pollard), and assistance in the field by Ann-Laure Moreau and Christopher Wilson. Reviews by Laurel Goodwin and an anonymous reviewer and help by Editor William Dunne were much appreciated.

References

Ahmadov, R., Aydin, A., Karimi-Fard, M., Durlofsky, L.J., 2007. Permeability upscaling of fault zones in the Aztec Sandstone, Valley of Fire State Park, Nevada with a focus on slip surfaces and slip bands. Hydrogeology Journal (Online First), doi:10.1007/s10040-007-0180-2.

Atkinson, B.K., 1987. Fracture Mechanics of Rocks. Academic Press, London.

Barenblatt, G.I., 1962. The mathematical theory of equilibrium cracks in brittle fracture. Advances in Applied Mechanics 7, 55–129.

Barquins, M., Petit, J.P., 1992. Kinetic instabilities during the propagation of a branch crack: effects of loading conditions and internal pressure. Journal of Structural Geology 14, 893–903.

Barquins, M., Petit, J.P., Maugis, D., Ghalayini, K., 1991. Path and kinetics of branching from defects under uniaxial and biaxial compressive loading. International Journal of Fracture 54, 139–163.

Bohannon, R.G., 1983. Mesozoic and Cenozoic tectonic development of the Muddy, North Muddy, and northern Black Mountains, Clark County, Nevada. In: Miller, D.M., Todd, V.R., Howard, K.A. (Eds.), Tectonic and Stratigraphic Studies in the Eastern Great Basin. Geological Society of America Memoir, 157, pp. 125–148.

Bohannon, R.G., Grow, J.A., Miller, J.J., Blank, R.H., 1993. Seismic stratigraphy and tectonic development of Virgin River depression and associated basins, southeastern Nevada and northwestern Arizona. Geological Society of America Bulletin 105, 501–520.

Bombolakis, E.G., 1973. Study of the brittle fracture process under uniaxial compression. Tectonophysics 18, 231–248.

Brace, W.F., Bombolakis, E.G., 1963. A note on brittle crack growth in compression. Journal of Geophysical Research 68, 3709–3713.

Bürgmann, R., Pollard, D.D., Martel, S.J., 1994. Slip distributions on faults: effects of stress gradients, inelastic deformation, heterogeneous host-rock stiffness, and fault interaction. Journal of Structural Geology 16, 1675–1690.

Çakir, M., Aydin, A., Campagna, D.J., 1998. Deformation pattern around the conjoining strike-slip fault systems in the Basin and Range, southeast Nevada: the role of strike-slip faulting in basin formation and inversion. Tectonics 17, 344–359.

Carpenter, D.G., Carpenter, J.A., 1994. Fold-thrust structure, synorogenic rocks and structural analysis of the North Muddy and Muddy Mountains, Clark County, Nevada. In: Dobbs, S.W., Taylor, W.J. (Eds.), Structural and Stratigraphic Investigations and Petroleum Potential of Nevada, with Special Emphasis South of the Railroad Valley Producing Trend. Nevada Petroleum Society Conference II, pp. 65–94.

Cartwright, J.A., Trudgill, B.D., Mansfield, C.S., 1995. Fault growth by segment linkage: an explanation for scatter in maximum displacement and trace length data from the Canyonlands Grabens of SE Utah. Journal of Structural Geology 17, 1319–1326.

Chaker, C., Barquins, M., 1996. Sliding effect on branch crack. Physics and Chemistry of the Earth 21, 319–323.

Cooke, M., 1997. Fracture localization along faults with spatially varying friction. Journal of Geophysical Research 102, 22425–22434.

Cotterell, B., Rice, J.R., 1980. Slightly curved or kinked cracks. International Journal of Fracture 16, 155–169.

Cowie, P.A., Scholz, C.H., 1992a. Displacement-length scaling relationship for faults: data synthesis and discussion. Journal of Structural Geology 14, 1149–1156.

Cowie, P.A., Scholz, C.H., 1992b. Physical explanation for the displacement-length relationship of faults using a post-yield fracture mechanics model. Journal of Structural Geology 14, 1133–1148.

Cruikshank, K.M., Zhao, G., Johnson, A.M., 1991. Analysis of minor fractures associated with joints and faulted joints. Journal of Structural Geology 13, 865–886.

Davatzes, N.C., Aydin, A., 2003. The formation of conjugate normal fault systems in folded sandstone by sequential jointing and shearing, Waterpocket monocline, Utah. Journal of Geophysical Research 108, 2478, doi:10.1029/2002JB002289.

Davatzes, N.C., Aydin, A., Eichhubl, P., 2003a. Overprinting faulting mechanisms during the development of multiple sets in sandstone, Chimney Rock fault array, Utah, USA. Tectonophysics 363, 1–18.

Davatzes, N.C., Aydin, A., Eichhubl, P., 2003b. Overprinting faulting mechanisms in high porosity sandstones of SW Utah. Journal of Structural Geology 25, 1795–1813.

Dawers, N.H., Anders, M.H., Scholz, C.H., 1993. Growth of normal faults: Displacement-length scaling. Geology 21, 1107–1110.

de Joussineau, G., Aydin, A., in press. The evolution of the damage zone with fault growth in sandstone and its multiscale characteristics. Journal of Geophysical Research (In Press).

Du, Y., Aydin, A., 1995. Shear fracture patterns and connectivity at geometric complexities along strike-slip faults. Journal of Geophysical Research 100, 18093–18102.

Dugdale, D.S., 1960. Yielding of steel sheets containing slits. Journal of the Mechanics and Physics of Solids 8, 100–104.

Eichhulb, P., Taylor, W.L., Pollard, D.D., Aydin, A., 2004. Paleo-fluid flow and deformation in the Aztec Sandstone at the Valley of Fire, Nevada—Evidence for the coupling of hydrogeologic, diagenetic and tectonic processes. Geological Society of America Bulletin 116, 1120–1136.

Engelder, T., 1993. Stress Regimes in the Lithosphere. Princeton University Press, NJ, USA.

Erdogan, F., Sih, G.C., 1963. On the crack extension in plates under plane loading and transverse shear. Journal of Basic Engineering 85, 519–527.

Fletcher, R.C., Pollard, D.D., 1981. Anticrack model for pressure solution surfaces. Geology 9, 419–424.

Flodin, E., Aydin, A., 2004a. Evolution of a strike-slip fault network, Valley of Fire State Park, southern Nevada. Geological Society of America Bulletin 116, 42–59.

Flodin, E., Aydin, A., 2004b. Faults with asymmetric damage zones in sandstone, Valley of Fire State Park, southern Nevada. Journal of Structural Geology 26, 983–988.

Flodin, E., Prasad, M., Aydin, A., 2003. Petrophysical constraints on deformation styles in Aztec Sandstone. Pure and Applied Geophysics 160, 1589–1610.

Flodin, E.A., Gerdes, M., Aydin, A., Wiggins, W.D., 2005. Petrophysical properties of cataclastic fault rock in sandstone. In: Sorkhabi, R., Tsuji, Y. (Eds.), Faults, fluid Flow, and Petroleum Traps. American Association of Petroleum Geologists Memoir, 85, pp. 197–227.

Granier, T., 1985. Origin, damping and pattern of development of faults in granite. Tectonics 4, 721–737.

Gupta, A., Scholz, C.H., 2000. A model of normal fault interaction based on observations and theory. Journal of Structural Geology 22, 865–879.

Hill, R., 1989. Analysis of deformation bands in the Aztec Sandstone, Valley of Fire State Park, Nevada. MS Thesis, Las Vegas University, University of Nevada.

Horii, H., Nemat-Nasser, S., 1983. Estimate of stress intensity factors for interacting cracks, in: Yuceoglu, U., Sierakowski, R.L., Glasgow, D.A. (Eds), Advances in Aerospace Structures, Materials and Dynamics. Proceedings of the ASME Symposium, pp. 111–117.

Horii, H., Nemat-Nasser, S., 1985. Compression induced microcrack growth in brittle solids: axial splitting and shear failure. Journal of Geophysical Research 90, 3105–3125.

Horii, H., Nemat-Nasser, S., 1986. Brittle failure in compression: splitting, faulting and brittle-ductile transition. Philosophical transactions of the Royal Society of London Series A. Mathematical and Physical Sciences 319, 337–374.

Ingraffea, A.R., 1987. Theory of crack initiation and propagation in rock. In: Atkinson, A.K. (Ed.), Fracture Mechanics of Rock. Academic Press, London, pp. 71–110.

Kattenhorn, S.A., Marshall, S.T., 2006. Fault-induced perturbed stress fields and associated tensile and compressive deformation at fault tips in the ice shell of Europa: implications for fault mechanics. Journal of Stuctural Geology 28, 2204–2221.

Kelly, P.G., Sanderson, D.J., Peacock, D.C.P., 1998. Linkage and evolution of conjugate strike-slip fault zones in limestones of Somerset and Northumbria. Journal of Structural Geology 20, 1477–1493.

Kim, Y., Peacock, D.C.P., Sanderson, D.J., 2003. Mesoscale strike-slip faults and damage zones at Marsalforn, Gozo Island, Malta. Journal of Structural Geology 25, 793–812.

Kim, Y., Peacock, D.C.P., Sanderson, D.J., 2004. Fault damage zones. Journal of Structural Geology 26, 503–517.

Liu, X., 1983. Perturbations de contraintes liées aux structures cassantes dans les calcaires fins du Languedoc: Observations et simulations mathématiques. 3rd Cycle Thesis, Université Montpellier II.

Mansfield, C., Cartwright, J., 2001. Fault growth by linkage: observations and implications from analogue models. Journal of Structural Geology 23, 745–763.

Martel, S.J., 1990. Formation of compound strike-slip fault zones, Mount Abbot quadrangle, California. Journal of Structural Geology 12, 869–877.

Martel, S.J., 1997. Effects of cohesive zones on small faults and implications for secondary fracturing and fault trace geometry. Journal of Structural Geology 19, 835–847.

Martel, S.J., Boger, W.A., 1998. Geometry and mechanics of secondary fracturing around small three-dimensional faults in granitic rocks. Journal of Geophysical Research 103, 21299–21314.

Martel, S.J., Pollard, D.D., Segall, P., 1988. Development of simple strike-slip fault zones, Mount Abbot quadrangle, Sierra Nevada, California. Geological Society of America Bulletin 100, 1451–1465.

McGrath, A.G., Davison, I., 1995. Damage zone geometry around fault tips. Journal of Structural Geology 17, 1011–1024.

Muskhelisvili, N.I., 1953. Some Basic Problems of the Mathematical Theory of Elasticity. Noordhoff Ltd, Groningen, The Netherlands.

Mutlu, O., Pollard, D.D., 2006. A complementarity approach for modeling fractures. The 41st U.S. Symposium on Rock Mechanics (USRMS): '50 Years of Rock Mechanics—Landmarks and Future Challenges', Golden Rocks, Colorado, June 17–21.

Myers, R., 1999. Structure and hydraulics of brittle faults in sandstone. PhD thesis, Stanford University.

Myers, R., Aydin, A., 2004. The evolution of faults formed by shearing across joint zones in sandstone. Journal of Structural Geology 26, 947–966.

Nemat-Nasser, S., Horii, H., 1982. Compression induced non planar crack extension with application to splitting, exfoliation and rock-burst. Journal of Geophysical Research 87, 6805–6821.

Nemat-Nasser, S., Horii, H., 1984. Rock failure in compression. International Journal of Engineering Sciences 22, 999–1011.

Peacock, D.C.P., 1991. Displacement and segment linkage in strike-slip fault zones. Journal of Structural Geology 13, 1025–1035.

Peacock, D.C.P., Sanderson, D.J., 1991. Displacement, segment linkage and relay ramps in normal fault zones. Journal of Structural Geology 13, 721–733.

Peacock, D.C.P., Sanderson, D.J., 1995. Pull-aparts, shear fractures and pressure solution. Tectonophysics 241, 1–13.

Petit, J.P., Barquins, M., 1988. Can natural faults propagate under mode II conditions? Tectonics 7, 1243–1256.

Petit, J.P., Mattauer, M., 1995. Paleostress superimposition deduced from mesoscale structures in limestone: The Matelles exposure, Languedoc, France. Journal of Structural Geology 17, 245–256.

Pollard, D.D., Segall, P., 1987. Theoretical displacements and stresses near fractures in rock: with applications to faults, joints, veins, dikes, and solution surfaces. In: Atkinson, B.K. (Ed.), Fracture Mechanics of Rocks. Academic Press, London, pp. 277–349.

Rispoli, R., 1981. Stress fields about strike-slip faults inferred from stylolites and tension gashes. Tectonophysics 75, 29–36.

Schlische, R.W., Young, S.S., Ackermann, R.V., Gupta, A., 1996. Geometry and scaling relations of a population of very small rift-related normal faults. Geology 24, 683–686.

Segall, P., Pollard, D.D., 1983. Nucleation and growth of strike-slip faults in granite. Journal of Geophysical Research 88, 555–568.

Schulson, E.M., 2002. On the origin of a wedge crack within the icy crust of Europa. Journal of Geophysical Research Planets 107, 5107–5116.

Sternlof, K.R., Rudnicki, J.W., Pollard, D.D., 2005. Anticrack inclusion model for compaction bands in sandstone. Journal of Geophysical Research 110, B11403, doi:10.1029/2005JB003764.

Taylor, W.L., Pollard, D.D., Aydin, A., 1999. Fluid flow in discrete joint sets: Field observations and numerical simulations. Journal of Geophysical Research 104, 28983–29006.

Willemse, E.J.M., Pollard, D.D., 1998. On the orientation and patterns of wing cracks and solution surfaces at the tips of a sliding flaw or fault. Journal of Geophysical Research 103, 2427–2438.

Wilson, G., 1960. The tectonics of the 'Great ice Chasm', Filchner Ice Shelf, Antarctica. Proceedings of the Geological Association of London 71, 130–138.

Wilkins, S.J., Schultz, R.A., 2005. 3-D cohesive end zone model for source scaling of strike-slip interplate earthquakes. Bulletin of the Seismological Society of America 95, 2232–2258.